

# Extreme Value Statistics of the Total Energy in an Intermediate Complexity Model of the Mid-latitude Atmospheric Jet.

## Part I: Stationary case.

Mara Felici,<sup>1,2,\*</sup> Valerio Lucarini,<sup>1</sup> Antonio Speranza,<sup>1</sup> and Renato Vitolo<sup>1</sup>

<sup>1</sup> *PASEF – Physics and Applied Statistics of Earth Fluids,  
Dipartimento di Matematica ed Informatica, Università di Camerino,  
Via Madonna delle Carceri, 62032 Camerino (MC), Italy*

<sup>2</sup> *Dipartimento di Matematica U. Dini, Università di Firenze,  
viale Morgagni 67/A – 50134 Firenze, Italy*

## Abstract

An intermediate complexity baroclinic model for the atmospheric jet at middle-latitudes is used as a stochastic generator of earth-like time series: in the present case the total energy of the system. Statistical inference of extreme values is applied to yearly maxima sequences of the time series, in the rigorous setting provided by extreme value theory. In particular, the Generalized Extreme Value (GEV) family of distributions is used here as a fundamental model for its simplicity and generality. Several physically realistic values of the parameter  $T_E$ , descriptive of the forced equator-to-pole temperature gradient and responsible for setting the average baroclinicity in the atmospheric model, are examined. Stationary time series of the total energy are generated and the estimates of the three GEV parameters – location, scale and shape – are inferred by maximum likelihood methods. Standard statistical diagnostics, such as return level and quantile-quantile plots, are systematically applied to assess goodness-of-fit. The location and scale GEV parameters are found to have a piecewise smooth, monotonically increasing dependence on  $T_E$ . This is in agreement with the similar dependence on  $T_E$  observed in the same system when other dynamically and physically relevant observables are considered. The shape parameter also increases with  $T_E$  but is always negative, as *a priori* required by the boundedness of the total energy of the system. The sensitivity of the statistical inference process is studied with respect to the selection procedure of the maxima: the roles of both the length of maxima sequences and of the length of data blocks over which the maxima are computed are critically analyzed. Issues related to model sensitivity are also explored by varying the resolution of the system.

PACS numbers: 02.50.Tt, 02.70.-c, 47.11.-j, 92.60.Bh, 92.70.Gt

---

\*Electronic address: mara.felici@math.unifi.it; URL: [www.unicam.it/matinf/pasef](http://www.unicam.it/matinf/pasef)

## **Contents**

<b>I. Introduction</b>	4
<b>II. Data and Methods</b>	8
A. Total Energy of the Atmospheric Model	8
B. Parameter Estimation and Model Assessment in GEV Inference	9
<b>III. GEV Inferences for 1000 Annual Maxima</b>	13
A. Smoothness of GEV Inferences with Respect to System Parameters	14
<b>IV. Sensitivity of the GEV inferences</b>	16
A. Sensitivity with Respect to the Extreme Events Sample Size	16
B. Sensitivity with Respect to the Extreme Events Selection Procedure: Soft Extremes	18
C. Sensitivity with Respect to the Model Resolution	19
<b>V. Summary and Conclusions</b>	21
<b>Acknowledgments</b>	23
<b>A. Classical Theory of Extreme Value Distributions</b>	24
<b>B. A Model for the Mid-Latitudes Atmospheric Circulation</b>	26
<b>References</b>	29

## I. INTRODUCTION

The study of climatic extreme events is of paramount importance for society, particularly in the fields of engineering and environmental and territorial planning. Indeed, temporal variations in the statistics of extreme events may have more acute and disruptive effects than changes in the mean climate [24]. In works of economical nature (see *e.g.* Nordhaus [39]), the special role played by the extreme events in terms of impacts is included with the hypothesis that the costs associated with climatic change can be represented as strongly nonlinear functions of the observed variations in surface temperature. This constitutes a clear motivation for which, when the impacts of climatic change are analyzed, the interest for variations in the statistics of extreme events plays a strategic role [15, 34].

In the scientific literature, some recent papers in which the existence of trends in the frequency of extreme (precipitation) events was pushed forward in quantitative terms are those by Karl *et al.* [22, 23]. Here the authors stated that the *percentage of the U.S.A. with a much above normal proportion of total annual precipitation from extreme precipitation events (daily events at or above 2 inches)* showed an increase from 9% in 1910-1920 to about 11% in the '90s. Despite severe scientific criticism to these papers by many other researchers in the field, the basic idea that the frequency of extreme events may change together with average surface temperature was discussed more and more and, eventually, it became one of the issues of analysis for the Intergovernmental Panel for Climate Change: a specific a specific report on *Changes in extreme weather and climate events* was issued in 2002 [16]. Basic questions, when dealing with extremes of complex processes, is: what is the correct way of measuring extremes? Are we concentrating on *local* or *global* fluctuations of the system in question? How do we measure local extremes? Extremes of wind speeds, of rainfall amounts, of economical damage? Moreover, the enhancement in the extreme events might be quantified either in terms of number of events, or in size of the average extreme event, or a combination thereof. Several other ambiguities make it often difficult to follow literature on the subject.

Overall, two important weaknesses of much work on the subject of extreme meteo-climatic events and of their trends are:

- the lack of interpretation of the dynamical mechanisms that should cause the hypothesized changes in the frequency of extremes of various nature; often such mechanisms are just alluded to instead of being explicitly formulated and analyzed;
- the lack of a common and theoretically founded definition of “extremes”.

The deficit in the first point above may negatively affect both deterministic and statistical

studies of the phenomena in question. One major example on global processes is that, despite the great attention attracted by the subject, very few researchers have investigated in detail the basic mechanisms that should associate an increased  $CO_2$  concentration to enhanced extreme weather events. The chain of mechanisms possibly linking  $CO_2$  concentration and weather extremes is too long even for an adequate qualitative discussion here, but we shall concentrate on the basic sequence: enhanced surface temperature  $\rightarrow$  enhanced baroclinicity  $\rightarrow$  changes in the upper tail of the probability distribution function of the baroclinic disturbances. But no robust analysis of this complex dynamical “chain” has been offered so far.

As for the second point above, the lack of a common rigorous framework for the statistical analysis of extremes (with few exceptions such as *e.g.* [25, 49, 50]) provides a serious drawback for the interpretation and comparison of results from different studies. Moreover, this problem is not even justified, since mathematical theories of extreme events are well-developed [3, 5, 8, 9, 10, 11, 29] and the derived methods are quite successful in many applications [25, 40, 49, 50]. One basic ingredient of the theory relies on Gnedenko’s theorem [11], which states that, under fairly mild assumptions, the distribution of the block-maxima of a sample of independent identically distributed variables converges to a family of three distinct distributions, the so-called Generalized Extreme Value (GEV) distributions. See Appendix A for a brief description. Notice that one of the earliest applications of this theory in the natural sciences occurred specifically in a meteorologic-climatic setting [20]. Other statistical models for extreme events include the  $r$ -largest statistics, threshold exceedance models such as the generalized Pareto distribution, and point processes, see [5].

The reliability of parametric estimates for extreme value models strongly depends on the asymptotic nature of extreme value theory. In particular, at least the following issues should be checked or addressed [5]:

1. *independence* of the selected extreme values;
2. using a *sufficiently large* number of extremes;
3. using values that are *genuinely* extreme.

Despite the importance of the third requirement, many studies actually deal with so-called *soft extremes* [26], which are maxima of too short data blocks or with too small return periods for the basic assumptions of the theory to hold. This is often the consequence of the limited amount of available data: on one hand, one has to restrict to maxima of data blocks, thereby discarding *most* available data; on the other hand one would like to have a *long* sequence of

extreme values. The net result is that the assumptions of the extreme value theorems often go unchecked and are sometimes plainly impossible to check, since the available climatic records cover at best the last century. Therefore, thinking in terms of annual maxima, in such cases we only have 100 extremes. The inevitable consequence of adapting the definition of extremes to the needs of the work is a serious reduction of reliability of the resulting estimates.

The goal of this paper is to infer and critically quality-check the statistical description of extreme values in the GEV distributions framework on the “earth-like” time series produced by a dynamical system descriptive of the mid-latitude atmospheric circulation featuring a chaotic regime. Such system has internally generated noise and can be effectively considered as a *stochastic generator* of data. Time series of the system’s total energy  $E(t)$  are used, which is a relevant global physical quantity. We analyze how the GEV distribution inferred from block maxima of  $E(t)$  depends on the value of the most important parameter of the system, namely the forced equator-to-pole temperature difference  $T_E$ , which controls the baroclinicity of the model. The reliability of the GEV fits is studied, by considering both shorter sequences of extremes and *soft extremes*. Moreover, issues related to model error and sensitivity are briefly examined by analyzing the effects of variations in model resolution. The use of numerically generated data allows us to avoid all the difficulties related to shortness of the available climatic records, such as missing observations and low-quality data. In particular, we do not need to worry about the wastage of data caused by the selection of annual maxima, which is a serious limitation when considering observational data. In such methodological sense, our approach is similar to that of [48] as far as statistical inference is concerned. However, an important difference is that the statistics of the time series  $E(t)$  generated by the atmospheric model *cannot be directly chosen*: there is no explicit formula relating the probability density function of the adopted observable and the parameter  $T_E$ . This problem we analyze elsewhere [35].

The structure of the paper is now outlined. In Sec. II we first describe the set-up of the numerical experiments performed with the atmospheric model and then the methods of statistical analysis of extreme values adopted for the total energy time series. The results for the considered reference case of 1000 yearly maxima are presented in Sec. III. Assessment of the sensitivity of the inferences is studied in Sec. IV, by varying the length of yearly maxima sequences, the block length over which maxima are taken, and the model resolution. The dependence of the GEV parameters with respect to  $T_E$  is also analyzed in this section. Sec. V summarizes the results and their relation with the above discussion. The theory and the methods of Extreme Value distributions, as far as needed in the present work, are briefly

reviewed in Appendix A. The model of the baroclinic jet used as a stochastic generator is described in Appendix B, referring to [35] for a thorough discussion.

## II. DATA AND METHODS

### A. Total Energy of the Atmospheric Model

We consider a quasi-geostrophic intermediate complexity model [35, 36, 46] (also see Appendix B), providing a basic representation of the turbulent jet and of the baroclinic conversion and barotropic stabilization processes which characterize the physics of the mid-latitudes atmospheric circulation. The model is relaxed towards a given equator-to-pole temperature profile which acts as baroclinic forcing. It features several degrees of freedom in the latitudinal direction and two layers in the vertical - the minimum for baroclinic conversion to take place [41, 44]. The system's statistical properties radically change when the parameter  $T_E$ , determining the forced equator-to-pole temperature gradient, is changed. In particular, as  $T_E$  increases a transition occurs from a stationary to an earth-like chaotic regime with internally generated noise. By chaotic, we mean that the system possesses a strange attractor in phase space [7]. For a detailed description of the model physics and dynamics see [35].

In the present setting, the model is used as a stochastic generator of earth-like time series for testing the reliability of different statistical approaches [48] and studying the dynamics of extremes [35]. A uniformly spaced grid of 21 values of the parameter  $T_E$  is fixed in the range  $[10, 50]$ , starting from 10 and increasing with step 2. The baroclinic model is run for  $T_E$  fixed at each of these values, producing 21 simulations of length 1000 years (preceded by an initial transient of five years) where the total energy  $E(t)$  is written every 6 hours. The formula of the total energy is given in Appendix B, equation (B15). We recall that, in the non-dimensionalization of the system,  $T_E = 1$  corresponds to  $3.5 K$ , 1 unit of total energy corresponds to roughly  $5 \times 10^{17} J$ , and  $t = 0.864$  is one day, see [35] for details.

For each of the selected values of  $T_E$ , a chaotic attractor is numerically detected in the phase space of the model. This is illustrated by the autocorrelations of the time series of the total energy  $E(t)$  (Fig. 1), which decay to zero on a time scale that is comparable with that of the atmospheric system (roughly 10-15 days [33]). Since all parameters of the model are kept fixed in each simulation, by discarding the initial transient, the time series of  $E(t)$  may be considered a realization of a stationary stochastic process.

The distribution of the total energy time series is visualized by means of the histograms and boxplots in Fig. 2, for three values of  $T_E$ . Notice that, as  $T_E$  increases,

- the upper tail of the distribution becomes heavier, whereas the lower tail shortens;
- both the average value and the variability of the total energy time series increase.



The latter point is clearly visualized in Fig. 3, where the time-averaged total energy is displayed for each of the 21 stationary time series, together with confidence intervals. Throughout the paper, confidence intervals are computed as average plus/minus sample standard deviation multiplied by 1.96.

In concluding this section a theoretical remark is in order here. All examined strange attractors are implicitly *assumed* to possess a unique Sinai-Ruelle-Bowen (SRB) ergodic invariant measure [7]. This is indeed a rather general and difficult problem in Dynamical Systems and Physics: on the one hand, existence of a unique SRB measure is *necessary* to rigorously associate a stationary stochastic process with the dynamical evolution law. On the other hand, existence of a unique SRB measure is a very strong regularity assumption for a dynamical system: in general it is even the question whether invariant measures exist at all and, if so, whether a finite or infinite number of invariant measures coexist for a given chaotic system. Moreover, even if an SRB measure exists and is unique, it is in general non-parametric: there is *no explicit formula* relating the statistical behavior to the system's equation and parameters.

## B. Parameter Estimation and Model Assessment in GEV Inference

As discussed in the previous section, the time series we work with are characterized by fast decay of autocorrelations, which implies weak (short time-range) dependence of the observations, compare Fig. 1. Inference of threshold exceedance models [5, 8, 29] is in this case complicated by the choices of suitable threshold values and cluster size for *declustering* (see *e.g.* [5, Chap. 5]), which might be somewhat arbitrary in the applications. On the other hand, since the dependence is short-range, maxima of the total energy time series, taken over sufficiently large data blocks, are with good approximation independent. This is why we have preferred the use of the GEV with respect to threshold models. Moreover, since we can generate time series of arbitrary length, for simplicity we refrained from using the  $r$ -largest statistics, which is often valid alternative to the GEV, especially when data scarcity is an issue. In this section, therefore, we recall the methods of GEV inference as far as needed in the present work. The exposition is largely based on [5]. Also see [3, 5, 8, 9, 10, 11, 29] for methodology and terminology of extreme value theory.

Gnedenko's theorem [11], or the *three types theorem*, first presented in a slightly less general form by Fisher and Tippet [9]) states that, under fairly mild assumptions, the distribution of the block-maxima of a sample of independent identically distributed variables converges, in

a suitable limit, to one of three types of extreme value distributions. The three types are in fact special cases of the GEV distribution (also called von Mises type), having the following expression:

$$G(x) = \exp \left\{ - \left[ 1 + \xi \left( \frac{x - \mu}{\sigma} \right) \right]^{-1/\xi} \right\} \quad (1)$$

for  $x$  in the set  $\{x : 1 + \xi(x - \mu)/\sigma > 0\}$  and  $G(x) = 0$  otherwise, with  $-\infty < \mu < +\infty$ ,  $\sigma > 0$ , and  $-\infty < \xi < +\infty$ . The quantities  $(\mu, \sigma, \xi)$  are called location, scale and shape parameter, respectively. In such a framework, statistical inference of extreme values amounts to estimating the GEV distributional parameters  $(\mu, \sigma, \xi)$  for a given time series and assessing the quality of the fit. If  $\xi > 0$  ( $\xi < 0$ ) the distribution is usually referred to as Fréchet (Weibull) distribution, if  $\xi = 0$  we have the Gumbel distribution, which can be expressed as (A5). See Appendix A for further theoretical details and [3, 5, 8, 10, 29] for examples and discussion.

In practical application of the extreme value theory the parent distribution function of the data is typically unknown. Therefore, both the type of limiting distribution and the parameter values must be inferred from the available data and the quality of the resulting estimates should always be assessed. For GEV inference, a sequence of maxima is constructed by subdividing the available data  $\{x_i\}$  into blocks of equal length and extracting the maximum from each block. The block length is one of the choices playing the usual, critical role between bias and variance in the parametric estimates. Too short blocks increase the length of the maxima sequence but, at the same time, they increase the risk of failure of the limit (A4). If the blocks are too long, the resulting scarcity of maxima induces an enhanced uncertainty of the inferred values of the GEV parameters. In many situations a reasonable (and sometimes compulsory) choice is to consider the annual maxima (see [5]).

Assume that the observations in the time series are equispaced in time and that none of them is missing (both conditions are often violated in concrete cases, see *e.g.* [40]). Let  $n$  be the number of observations in a year and denote by  $M_{n,1}, \dots, M_{n,m}$  the sequence of the annual maxima, *i.e.*, the maxima over data blocks of length  $n$ . Under the assumption of independence of the  $X_n$ , the variables  $M_{n,1}, \dots, M_{n,m}$  are independent as well. In fact, approximate independence of the  $M_{n,i}$  holds also in the case of *weak dependent* stationary sequences, see [5, 29] for definitions and examples.

Among the numerous methods to infer the GEV parameters (graphical or moment-based techniques, see [3]), we adopt the maximum likelihood estimator for its great adaptability to changes of models. Denote by  $\boldsymbol{\theta} = (\mu, \sigma, \xi)$  the parameter vector for the GEV density  $g(x; \boldsymbol{\theta})$ , the latter being the derivative of  $G(x) = G(x; \boldsymbol{\theta})$  in (1). In the stationary context, the *block*

*maxima* of the observed data are assumed to be realizations of a stationary stochastic process having density  $g(x; \boldsymbol{\theta}^0)$ , where  $\boldsymbol{\theta}^0$  is the unknown parameter vector. The *maximum likelihood estimator*  $\hat{\boldsymbol{\theta}}^0$  of  $\boldsymbol{\theta}^0$  is defined as the value that maximizes the likelihood function

$$L(\boldsymbol{\theta}) = \prod_{i=1}^n g(M_{n,i}; \boldsymbol{\theta}). \quad (2)$$

In loose words, maximizing  $L(\boldsymbol{\theta})$  yields the parameter values for which the probability of observing the available data is the highest. It is often more advantageous to maximize the *log-likelihood function*

$$l(\boldsymbol{\theta}) = \log L(\boldsymbol{\theta}) = \sum_{i=1}^m \log g(M_{n,i}; \boldsymbol{\theta}) \quad (3)$$

and, according to (1), we get

$$\begin{aligned} l(\mu, \sigma, \xi) = \\ = \begin{cases} -m \log \sigma - \left(1 + \frac{1}{\xi}\right) \sum_{i=1}^m \left\{ \log \left[ 1 + \xi \left( \frac{M_{n,i} - \mu}{\sigma} \right) \right] - \left[ 1 + \xi \left( \frac{M_{n,i} - \mu}{\sigma} \right) \right]^{-\frac{1}{\xi}} \right\}, & \text{if } \xi \neq 0, \\ -m \log \sigma - \sum_{i=1}^m \left\{ \left( \frac{M_{n,i} - \mu}{\sigma} \right) - \exp \left[ - \left( \frac{M_{n,i} - \mu}{\sigma} \right) \right] \right\}, & \text{if } \xi = 0, \end{cases} \end{aligned} \quad (4)$$

defined on the points  $M_{n,i}$  that, in the case  $\xi \neq 0$ , satisfy the condition  $1 + \xi \left( \frac{M_{n,i} - \mu}{\sigma} \right) > 0$  for all  $i = 1, \dots, m$ . Indeed, since the logarithm is a monotonic increasing function, the likelihood function reaches its maximum value at the same point as the log-likelihood function.

Approximate confidence intervals for  $\hat{\boldsymbol{\theta}}^0$  are constructed using the fact that each component of  $\hat{\boldsymbol{\theta}}^0 = (\hat{\theta}_1^0, \hat{\theta}_2^0, \hat{\theta}_3^0) = (\hat{\mu}^0, \hat{\sigma}^0, \hat{\xi}^0)$  is asymptotically normal [5]:

$$\hat{\theta}_i^0 \sim N(\theta_i^0, \hat{\psi}_{i,i}) \quad \forall i = 1, \dots, d, \quad (5)$$

where  $\hat{\psi}_{i,j}$  is a generic element of the inverse of the *observed information matrix*  $I_0(\boldsymbol{\theta})$  defined by

$$I_0(\boldsymbol{\theta}) = \left( -\frac{\partial^2 l(\boldsymbol{\theta})}{\partial \theta_i \partial \theta_j} \right)_{i,j} \quad \forall i, j = 1, \dots, d \quad (6)$$

and evaluated in  $\boldsymbol{\theta} = \hat{\boldsymbol{\theta}}^0$ . From Eq. (5) one obtains the  $(1 - \alpha)$ -confidence interval for  $\hat{\theta}_i^0$ :

$$\theta_i^0 \pm z_{\frac{\alpha}{2}} \sqrt{\hat{\psi}_{i,i}} \quad (7)$$

where  $z_{\frac{\alpha}{2}}$  is the  $(1 - \alpha/2)$  quantile of the standard normal distribution. All confidence intervals in this paper are computed by formula (7), except when a more detailed analysis is presented. For example, in the assessment of inference quality, confidence intervals are also computed by a standard bootstrap procedure (applied to the sequence of annual maxima) and

by profile likelihood. The latter technique consists in the following. Consider the parameter  $\xi$ , to fix ideas. The profile likelihood of  $\xi$  is obtained by setting  $\mu$  and  $\sigma$  to their maximum likelihood estimates,  $\hat{\mu}^0$  and  $\hat{\sigma}^0$ , respectively, in the log-likelihood function  $l$  (4). The plot of  $l(\hat{\mu}^0, \hat{\sigma}^0, \xi)$  as a function of  $\xi$  is a section of the likelihood surface of (4) as viewed from the  $\xi$ -axis. Confidence intervals constructed from this graph are often more accurate than those obtained by observed information matrix, see [5] for examples.

One of the main goals of extreme value theory is estimating the probability of occurrence of events that are *more extreme* than those that have been observed thus far. Let  $z_p$  be the value that has a probability  $p$  to be exceeded every year by the annual maximum:  $P\{M_{n,i} > z_p\} = p$  with  $0 < p < 1$ . In common terminology  $z_p$  is called the *return level* associated with the *return period*  $1/p$ . A maximum likelihood estimator for  $z_p$  is obtained by plugging the estimates for  $\hat{\theta}^0 = [\hat{\mu}, \hat{\sigma}, \hat{\xi}]$  into the quantiles of  $G(x)$ , obtained by inverting Eq. (1). This yields the estimator

$$\hat{z}_p = \begin{cases} \hat{\mu} - \frac{\hat{\sigma}}{\hat{\xi}} \left[ 1 - \{-\log(1-p)\}^{-\hat{\xi}} \right] & \text{for } \hat{\xi} \neq 0, \\ \hat{\mu} - \hat{\sigma} \log \{-\log(1-p)\} & \text{for } \hat{\xi} = 0. \end{cases} \quad (8)$$

The variance of the return level estimator  $\hat{z}_p$  is approximated as

$$\text{Var}(\hat{z}_p) \approx \nabla z_p^T V \nabla z_p, \quad (9)$$

where  $\nabla z_p^T = \left[ \frac{\partial z_p}{\partial \mu}, \frac{\partial z_p}{\partial \sigma}, \frac{\partial z_p}{\partial \xi} \right]$ ,  $V$  is the variance-covariance matrix:

$$V(\mu, \sigma, \xi) = \begin{pmatrix} \text{Var}(\mu) & \text{Cov}(\mu, \sigma) & \text{Cov}(\mu, \xi) \\ \text{Cov}(\sigma, \mu) & \text{Var}(\sigma) & \text{Cov}(\sigma, \xi) \\ \text{Cov}(\xi, \mu) & \text{Cov}(\xi, \sigma) & \text{Var}(\xi) \end{pmatrix}, \quad (10)$$

and both  $\nabla z_p$  and  $V$  are evaluated at the maximum likelihood estimate  $\hat{\theta}^0 = [\hat{\mu}, \hat{\sigma}, \hat{\xi}]$ . This allows the construction of confidence intervals for  $\hat{z}_p$  and is referred to as the *delta method*. Again, profile likelihood and a bootstrap technique are used for goodness-of-fit assessment of the return level inferences.

Only for Weibull distributions ( $\xi < 0$ ) it is possible to have  $p = 0$ , corresponding to a return level with an infinite return period. In this case,

$$z_0 = \hat{\mu} - \frac{\hat{\sigma}}{\hat{\xi}}. \quad (11)$$

All information about the return levels is usually reported in the *return level plot*, where  $\hat{z}_p$  is plotted against  $\log y_p$ , where  $y_p = -\log(1-p)$  (compare Eq. (8)). The return level plot is linear for the Gumbel distribution, concave for  $\xi > 0$  (Fréchet) and has the horizontal

asymptote (11) (Weibull). Notice that the smallest values of  $p$  are usually those of interest, since they correspond to very rare (particularly extreme) events. In the return level plots, events with a short return period (large probability  $p$ ) are compressed near the origin of the axes, while outliers and rare events (small  $p$ ) are highlighted. For this reason such plots are very useful tools for both model analysis and diagnosis.

The above procedures for the estimates of return levels and GEV parameters require assessment with reference to the available data. Useful graphical checks are the *probability plot*, the *quantile-quantile plot* (QQ plot) and the return level plot. The first is the comparison between the estimated and the empirical distribution function  $\tilde{G}(x)$ . The latter is a stepfunction defined by

$$\tilde{G}(M_{(i)}) = \frac{i}{m+1}, \quad (12)$$

where  $M_{(i)}$  is the order statistics for the sequence  $M_{n,1}, \dots, M_{n,m}$  of  $m$  block maxima. Notice that the definition of the empirical d.f. (12) is not unique, see [3].

The QQ-Plot, formed by the points

$$\left\{ \left( \tilde{G}^{-1} \left( \frac{i}{m+1} \right), m_{(i)} \right), \quad \forall i = 1, \dots, m \right\} \quad (13)$$

highlights the behavior of the model tail, which is often the most interesting part. Substantial departures of the above plots from the diagonal indicate inadequacy of the GEV model or other systematic errors. Another diagnostic plot is constructed by adding confidence intervals for  $\hat{z}_p$  and return levels of the empirical d.f., according to Eq. (13), to the return level plot (see above). Agreement of the empirical d.f. with the return level curve suggests goodness of fit and adequacy of the GEV model.

All computations and plots in this paper have been made with the software **R** [14], available under the GNU license at [www.r-project.org](http://www.r-project.org). The library **ismev** ([www.cran.r-project.org](http://www.cran.r-project.org)), which is an **R**-port of the routines written by Stuart Coles as complement to [5], has been used with minor modifications.

### III. GEV INFERENCES FOR 1000 ANNUAL MAXIMA

The annual maxima are extracted from the 6-hourly time series of the energy described in Sec. II. Each series contains  $4 \times 365 \times 1000 = 1460000$  data. We then set  $n = 1460$  in (A1), thereby obtaining sequences of 1000 annual extremes of the total energy. The yearly maxima are linearly uncorrelated (Fig. 4), suggesting that it is safe and reasonable to assume independence. Also compare with the autocorrelation decay time in Fig. 1

On theoretical grounds we can at least deduce one constraint on the distribution of extremes for the energy time series. Indeed, since the attractor is contained within a bounded domain of the phase space and since the energy observable  $E(t)$  defined in (B15) is a continuous function of the phase space variables, it turns out that the total energy is bounded on any orbit lying on (or converging to) the attractor. Therefore, the energy extremes are *necessarily* Weibull distributed ( $\xi$  is negative). This provides a theoretically founded criterion for quality assessment of the obtained GEV inferences.

The GEV parameters  $(\mu, \sigma, \xi)$  are estimated by the maximum likelihood method (see Sec. II B) from the sequences of yearly maxima. The fitted values of  $(\mu, \sigma, \xi)$ , together with confidence bands (computed by the observed information matrix, formula (7)) are plotted as functions of  $T_E$  in Fig. 5. The inferred parameters  $\mu$  and  $\sigma$  increase monotonically with  $T_E$ . Estimates of  $\xi$  are in each case negative and the related confidence intervals are markedly bounded away from zero: observed information matrix, profile likelihood and bootstrap yield similar estimates. The latter result matches quite well the theoretical expectation discussed in the previous section. Also notice that the uncertainty in  $\xi$  may reach up to 21% of its value, whereas the parameters  $\mu$  and  $\sigma$  are quite accurately estimated: the maximal uncertainties in  $\mu$  and  $\sigma$  are 0.1% and 2.5% of the corresponding value, respectively.

Information on the tails of the energy distribution is straightforwardly expressed by the return level plots, where  $z_p = G^{-1}(1 - 1/p)$  is the return level associated to the  $p$ -year return period and  $G$  is the GEV distribution (1). In Fig. 6, return levels with return periods of 10, 100 and 1000 years are plotted as functions of  $T_E$ . Each graph is monotonically increasing with  $T_E$  and, for  $T_E$  fixed, the return levels increase with the return period.

The dependence of the GEV probability density with respect to  $T_E$  is illustrated in Fig. 7. The increase of scale and location parameters with  $T_E$  induces a rightward shift and a spread of the probability density. In particular, from the geophysical point of view, both the range and severity of possible extreme values of the total energy increase with  $T_E$ . In fact, this behavior sets in for  $T_E$  right after the creation of the chaotic attractor, see Fig. 7 right.

#### A. Smoothness of GEV Inferences with Respect to System Parameters

The dependence from  $T_E$  of the time-averaged total energy and of the inferred GEV parameters (including the return levels) is rather smooth, see Fig. 3 and Fig. 5. This strongly suggests the existence of functional relations of the form

$$\mu = \alpha T_E^\gamma \quad \text{and} \quad \sigma = \alpha' T_E^{\gamma'}. \quad (14)$$

Such power laws are fitted to the graphs of  $\mu$  and  $\sigma$  as follows.

To set ideas, we consider  $\mu$  and denote by  $\hat{\mu}(T_E^j)$  and  $\sigma_{\hat{\mu}}(T_E^j)$  the maximum likelihood estimate of  $\mu$  and the related standard deviation (calculated by the observed information matrix), respectively, where  $T_E^j$  is one of the 21 chosen values in the interval  $[10, 50]$ . A bootstrap procedure is performed where iterated realizations of a sequence of 21 independent Gaussian variables with mean  $\hat{\mu}(T_E^j)$  and standard deviation  $\sigma_{\hat{\mu}}(T_E^j)$  are simulated. For each realization, a power law fit as in (14) is performed. The sample average and standard deviation of the so obtained fits, constructed independently for  $\mu$  and  $\sigma$ , are reported in Tab. I and Tab. II.

Two distinct ranges of  $T_E$  are identified, where  $\mu$  scales by a different exponent, also see Fig. 8 left. For  $T_E \lesssim 18$   $\gamma_\mu$  is  $\sim 1.73$  while it decreases to  $\sim 1.6$  for  $T_E \gtrsim 18$ . The time-mean total energy of the system has a rather similar power-law dependence on  $T_E$  [35]. In the upper  $T_E$ -range the exponent of the power law of the extremes is larger than that of the time-mean total energy ( $\sim 1.52$ ), which implies that asymptotically the extremes tend to become relatively *more extreme*. When considering  $\sigma$ , there is an initial interval of  $T_E$  where no power law is obeyed, see Fig. 9 left. For  $22 \gtrsim T_E \gtrsim 15$   $\gamma_\sigma$  is  $\sim 3.0$  while it decreases to  $\sim 2.1$  for  $T_E \gtrsim 22$ . Since  $\gamma_\sigma > \gamma_\mu$  for high values of  $T_E$ , we have that asymptotically with  $T_E$  the spread of the maxima tends to become consistent with respect to their average location, thus suggesting a larger variability in the maxima. Shorter yearly maxima sequences, of length 300 and 100, lead to nearly identical estimates for both  $\gamma_\mu$  and  $\gamma_\sigma$  and their confidence intervals, thus implying that this is a rather robust property of the system.

Apart for the total energy, it turns out that analogous power law dependence with respect to  $T_E$  is detected in the considered model for several dynamical and physical observables, such as Lyapunov dimension, maximal Lyapunov exponent and average zonal wind [35]. This suggests that the whole attractor of the model (more precisely, its SRB measure) has some scaling laws with respect to  $T_E$ . The qualitative features described above for  $T_E$  sufficiently large, such as the form of  $(\mu, \sigma)$  as functions of  $T_E$  and the fact that  $\xi$  seems to approach a constant negative value, are most probably related to this scaling behavior. An important question we address elsewhere is whether this is a peculiarity of the baroclinic model used here or if analogous smoothness properties are common (*generic* or *robust* in some sense) for models of atmospheric dynamics, including General Circulation Models.



#### IV. SENSITIVITY OF THE GEV INFERENCES

The length of 1000 for the sequences of yearly maxima turns out to yield good accuracy for the GEV inferences. The sensitivity of such results has been tested by relaxing the experimental conditions considered in the previous section. This has been done in several ways:

- by varying the *number of extreme events* (length of the sequences of yearly maxima);
- by using *soft extremes* (maxima are computed over data blocks corresponding to time spans shorter than one year).
- by varying the resolution of the model.

The best estimates and related uncertainties of the GEV parameters obtained under modified experimental conditions have been first compared at phase value to what obtained in the reference case, in order to detect mismatch due to biases and changing precision. Moreover, the resulting differences in the GEV distributions have been inspected also with by adopting the standard graphical diagnostics, such as quantile-quantile and return level plots, and by computing bootstrap confidence intervals and profile likelihood both for the critical parameter  $\xi$  and for the return levels.

##### A. Sensitivity with Respect to the Extreme Events Sample Size

We describe what is found when reducing the number of yearly maxima used for GEV inference. The, particularly unfortunate, case occurring for  $T_E = 32$  is first analyzed by means of profile likelihood for the GEV parameter  $\xi$ . Sequences of 1000, 300, 100, and 50 yearly maxima of the total energy are used to produce the plots in Fig. 10. The cases 1000, 300, and 100 yield coherent estimates for  $\xi$ . For detailed diagnostics, confidence intervals are computed by the observed information matrix (formula (7)) and compared by those obtained by profile likelihood and by a standard bootstrap procedure. The three methods yield similar results in all cases, both for the estimates and for the confidence intervals. However, for 50 maxima the confidence intervals become very wide and a positive value for  $\xi$  is inferred, which is unphysical.

The decay of the inference quality is revealed in a different way by the profile likelihood plots for the 100-year return levels (Fig. 11). It is, in general, not quite safe to infer, from a series of  $n$  annual extremes, return levels with return periods larger than  $n$  years. Extrapolation



to larger return periods may produce incorrect values and is likely to yield significant uncertainties. For the considered case, the estimates are coherent for 1000, 300, and 100 yearly maxima. As expected, the confidence intervals (computed by the  $\delta$  method, see Sec. II B) become larger as shorter sequences of maxima are used. This also holds for bootstrap and profile likelihood. However, for 50 maxima the profile likelihood confidence intervals become very skewed as opposed to bootstrap or  $\delta$  method. This clearly indicates poor approximation of normality for the GEV estimators [5], revealing the intrinsic unreliability of the estimates.

Quantile-quantile and return level plots for the above inferences are reported in Fig. 12. These confirm excellent quality for 1000, 300, and 100 maxima, whereas they reveal that something must be wrong for 50. In the quantile-quantile plots (top row of Fig. 12), from left to right there appear increasing departures from the diagonal in the tails, especially the upper tail, whereas the central part of the distribution does not suffer from sample reduction, except in the case of 50 maxima. Analogous effects occur in the upper tail of the return level plots. The main point here is that the most delicate part of an extreme value inference is the behavior of the tails. Usually, this is also the aspect one is most interested in. Notice how the black line in the middle of the return level plot for 50 maxima erroneously suggests unboundedness of the return levels (which is only possible for  $\xi \geq 0$ , see Sec. II B). Therefore, extrapolations to high levels should be avoided in this case.

We emphasize that the value of  $T_E$  just examined corresponds to a particularly *bad* inference for 50 years. An overview, throughout the considered range of  $T_E$ , of GEV inference sensitivity to length reduction is summarized in Fig. 13, where the cases of 300, 100, 50 yearly maxima are plotted against 1000. The quality of the fits, of course, generally decreases when using shorter series of maxima. Inference of  $\xi$  is particularly sensitive to the length of the series of maxima: the maximal value of the ratios between uncertainty in  $\xi$  and value of the corresponding maximum likelihood estimate of  $\xi$  is 600%, 1387%, 45%, and 21%, for 50, 100, 300, and 1000 maxima, respectively. The median of those ratios is 48%, 30%, 19%, 10%, respectively. Taking only 50 maxima yields two positive estimates of  $\xi$  (for  $T_E = 32$  and 50), which is an unphysical result, and overall very large uncertainties: for many values of  $T_E$ , confidence bands for  $\xi$  include part of the positive axis. The bias in the estimates of  $\xi$  induces a significant alteration in those of  $\sigma$ , although the inferred values of  $\mu$  remain quite stable. Also notice the big uncertainties in the return levels for the two cases  $T_E = 32$  and 50, corresponding to positive estimates of  $\xi$ .

If we further consider additional sources of difficulty present in nature (for example the annual seasonal modulation), skepticism with respect to several inferences on extremes proposed

in meteo-climatic literature seems justified.

## B. Sensitivity with Respect to the Extreme Events Selection Procedure: Soft Extremes

We now turn to the second type of inference sensitivity mentioned above, obtained by using so-called *soft extremes* [26] instead of *genuine* extremes. In the present setting, we simulate the usage of *soft extremes* by considering sequences of maxima over data blocks that correspond to time spans shorter than one year, in particular 0.6, 1.2, and 3 months. In the first two cases, and especially in the first, we are not even sure that the considered maxima are effectively uncorrelated, which is the typical situation in real systems. In each case, the number of considered extremes is kept fixed to 1000, so that the difference is only determined by block length.

The net result of using shorter time spans is the introduction of a progressively larger bias in the GEV inferences. The location and shape parameters are systematically underestimated. For the location parameter  $\mu$  (leftmost column in Fig. 14) the underestimation increases when taking maxima over shorter time-spans, but it also increases with  $T_E$ . Notice that this is quite different from the effect of reduction of the number of maxima, compare Fig. 13 (leftmost column). The sample medians of the relative differences between the estimates of  $\mu$  for 12 months and those for 3, 1.2, and 0.6 months (where the sample is indexed by the values of  $T_E$  for which the estimates are computed) are 3.2%, 5.7%, and 7.5% for 3, 1.2, and 0.6 months, respectively. Due to the definition of  $z_p$ , see (8), the underestimation of the 100-year return levels is a consequence of that of  $\mu$ . Also notice that the variations in the return levels connected to increase in  $T_E$  are much larger than those induced by usage of either soft extremes or shorter data sets, also compare with Fig. 13 (rightmost column). Conversely, the scale parameter  $\sigma$  (second column from left in Fig. 14) is *largely* overestimated: the sample median of the relative differences between the estimates of  $\sigma$  are 31%, 59%, and 82% for 3, 1.2, and 0.6 months, respectively. So in our case, taking soft extremes mistakingly suggests an enhanced variability in the extreme values.

Qualitatively, the response of the GEV estimates to the usage of *soft extremes* is explained by the introduction of much more data in the central part and in the lower tail of the distribution of the selected extreme values. From this fact, the underestimation of  $\mu$  follows directly. Moreover, since the range of the extreme events distribution gets wider, a larger variability is *artificially* introduced and this is indicated by an overestimated scale parameter

$\sigma$ . Lastly, the upper tail of the so obtained distribution of extremes looks more *squeezed*, given the wider extension at lower values. This corresponds to a more negative value of  $\xi$ , compare the third column from left in Fig. 14.

### C. Sensitivity with Respect to the Model Resolution

In this section we analyze the response of the GEV inferences to variations in the model. In fact, this question is a further aspect of the smoothness and robustness issues discussed in Sec. III A, which is of great practical importance: we would not like our estimates to drastically change if the model is slightly altered. Different choices are possible, such as introducing an orography in the bottom layer or changing the lateral boundary conditions. In the present setting, however, we confine ourselves to compare simulations of the baroclinic model computed at different resolutions (*i.e.*, with different spectral discretization order  $JT$ , see (B11)-(B14)).

In particular, time series of the total energy, of length 1000 years, are computed with the baroclinic model using four different resolutions:  $JT = 8, 16, 32, 64$  (resolution  $JT = 32$  is used throughout the rest of this paper). In each case the GEV parameters are estimated from sequences of 1000 yearly maxima. The results are compared with each other in Fig. 15. The relative differences of the estimated values of  $\mu$  between the case  $JT = 32$  and each of the other three cases (panel (A)) remain rather small: they are less than 1.5% for  $JT = 16$  and 64 and grow up to about 4% for  $JT = 8$ . Also the estimates of  $\xi$  in general agree quite well for all the considered resolutions.

More pronounced differences appear in the inferred values of the scale parameter  $\sigma$ : for  $T_E \geq 26$ , the estimates obtained with resolutions  $JT = 8$  and 64 are larger than those for  $JT = 16$  and 32. The estimates for  $\mu$  closely reflect the behavior of the time-averaged the total energy (computed on the same time series from which the yearly maxima are extracted). Considering, to fix ideas, the range  $T_E \in [26, 36]$ , for each fixed  $T_E$  both the inferred values of  $\mu$  and the time-averaged total energy (not shown) *decrease* as  $JT$  increases. Conversely, there is no simple relation between the sample standard deviation  $\sigma_E$  of the total energy time series and the GEV scale parameter  $\sigma$ : for the mentioned values of  $T_E$ , the sample standard deviation  $\sigma_E$  decreases for larger  $JT$  (not shown), whereas this is not so for the scale parameter, see above.

Power law fits of  $\mu$  and  $\sigma$  as functions of  $T_E$  are performed for 1000 yearly maxima of the total energy, where the baroclinic model is run with four different resolutions:  $JT = 8, 16,$

32, 64. As in Sec. III A, the range of  $T_E$  is divided into two intervals for the fits of  $\mu$  and into three for  $\sigma$  (in the latter case, no power law is found in the leftmost interval). Remarkable accuracy and coherence of the laws for  $\mu$  is observed. There is more variability in the power laws for  $\sigma$ , although again a striking coherence is observed for large  $T_E$ .

Summarizing, we have observed no dramatic model sensitivity for the GEV estimates. However, it is to be emphasized that a particularly *stable* observable has been examined here (the total energy) and only one type of model alteration has been considered, namely a change in the spectral resolution. We believe, though, our results are quite “generic” for the class of models considered in this paper.

## V. SUMMARY AND CONCLUSIONS

In this paper we have performed statistical inference of extreme values on time series obtained by means of a dynamically minimal two-level quasi-geostrophic model of the atmosphere at mid-latitudes. The physical observable used to generate the time series is the total energy of the system and the statistical model for the extremes is the Generalized Extreme Value distribution (GEV). Several physically realistic values of the parameter  $T_E$ , descriptive of the forced equator-to-pole temperature gradient and responsible for setting the average baroclinicity in the atmospheric model, are examined. In the standard setting, the maxima of the total energy are computed over one year long data blocks, and 1000 maxima are used as basis for the inference.

A result of the present investigation, having potential relevance in atmospheric dynamics, is the detection of a piecewise smooth dependence of the location and scale GEV parameters  $(\mu, \sigma)$  on the model parameter  $T_E$  controlling average baroclinicity. Two distinct power-laws, holding in different intervals of  $T_E$ , are obtained both for  $\mu$  and for  $\sigma$  as functions of  $T_E$ , where the fit for  $\mu$  is quite accurate. This regularity is put in relation with the results in [35], where analogous scaling laws are found for other dynamical indicators, such as Lyapunov exponents and dimension, and physical observables, such the time-space average of total energy and zonal wind. The shape parameter  $\xi$  also increases with  $T_E$  but is always negative, as *a priori* required by the boundedness of the total energy of the system. We conjecture that also the dependence of  $\xi$  on  $T_E$  becomes smooth when much longer time series are considered. All these problems will be further explored in connected work.

After the assessment of the goodness-of-fit by means of standard statistical diagnostics, such as return level and quantile-quantile plots and computation of confidence intervals by different procedures, we have consistently verified that:

- the selected block length of one year guarantees that the extremes are uncorrelated and genuinely extreme; guaranteeing this property may result more problematic when dealing with real observations because of seasonal modulations, etc.;
- the considered length of the series of maxima (1000 data) yields reliable parameter estimates;
- the GEV inferences are not dramatically affected by structural changes in the atmospheric model adopted in the present work.

The sensitivity of the statistical inference process is first studied with respect to the selection

procedure of the maxima: we analyze the effects of reducing either the length of maxima sequences or the length of data blocks over which the maxima are computed.

The first point is checked by repeating the GEV inferences with sequences of maxima having lengths 300, 100, and 50 years. The estimates are coherent for 1000, 300, and 100 yearly maxima, but the confidence intervals of the best estimates, not surprisingly, widen up as shorter sequences of maxima are used. Moreover, markedly unreliable estimates are obtained when only 50 yearly maxima are considered: the estimated long-term return levels are patently wrong, the uncertainty of the inferred shape parameter  $\xi$  is very large, and the best estimate of  $\xi$  is positive (that is, unrealistic) for a few values of  $T_E$ .

In order to address the second point, we have taken maxima over data blocks corresponding to shorter time spans, to explore the effects of using *soft extremes* [26]. Specifically, the sensitivity of the GEV inferences is analyzed with respect to shortening the length of the data blocks to 3, 1.2, and 0.6 months. The obtained statistics is “polluted”: a bias is introduced which is unacceptable for the cases of 1.2 and 0.6 months and still significant (at least for the GEV parameter  $\sigma$ ) for 3 months. Moreover, the parameter  $\xi$  tends to be underestimated. Taking shorter maxima sequences results in even larger uncertainties, very large for the case of 50 yearly maxima. Physically unrealistic values of  $\xi$  may also be obtained.

Lastly, issues related to model sensitivity are also explored by varying the (spectral) resolution of the system. It turns out that the GEV estimates are in general rather robust under this sort of perturbation. Summarizing, to get a good inference *many* maxima are required and they must be *genuinely extreme*, that is, taken over sufficiently large data blocks. Failing to fulfill these requirements may result in affecting the GEV inferences much more critically than adopting a baroclinic model with lower resolutions.

We conclude by highlighting that the parameterization of physical observables with respect to an external forcing is indeed a rather general and difficult problem in the dynamical analysis of the physical system. Existence of a unique Sinai-Ruelle-Bowen measure is *required* to rigorously associate a stationary stochastic process to the dynamical evolution law. However, even if an SRB measure exists and is unique, typically there is no explicit expression in terms of the system’s equations and parameters [7].

In this respect, the simplicity and the universality of the GEV model can be exploited to characterize chaotic systems by focusing on extreme values of suitable time series, rather than examining the distribution of all states visited by the system in phase space. Different model variants (both in boundary conditions and in model structure) and other observables and will be considered in future research.

## **Acknowledgments**

The authors wish to thank Stefano Pittalis for useful conversations. This work has been supported by MIUR PRIN Grant "Gli estremi meteo-climatici nell'area mediterranea: proprietà statistiche e dinamiche", Italy, 2003.

## APPENDIX A: CLASSICAL THEORY OF EXTREME VALUE DISTRIBUTIONS

Let  $X_1, \dots, X_n$  be a sequence of independent and identically distributed random variables (i.i.d.r.v.) where  $F_X$  is the common distribution function (d.f.). The classical theory of Extreme Values deals with the statistical behavior of the random variables

$$M_n = \max\{X_1, \dots, X_n\}, \quad (\text{A1})$$

which is the *maximum* of the first  $n$  variables (an analogous theory for the minima is developed similarly, since  $\min\{X_1, \dots, X_n\} = -\max\{-X_1, \dots, -X_n\}$ ). Under the assumptions of statistical independence and distributional equality of the  $X_i$ , we know that

$$P\{M_n \leq x\} = P\{X_1 \leq x, \dots, X_n \leq x\} = P\{X_1 \leq x\} \cdot \dots \cdot P\{X_n \leq x\} = F_X^n. \quad (\text{A2})$$

However, in most practical applications this property is useless because, typically  $F_X$  is unknown. Moreover, the limit of  $F_X^n$  is degenerate, since it is concentrated on the point  $x_+ = \sup\{x : F(x) < 1\}$ :

$$\lim_{n \rightarrow +\infty} F_X^n(x) = \begin{cases} 0 & x < x_+, \\ 1 & x \geq x_+. \end{cases} \quad (\text{A3})$$

This difficulty is avoided by assuming the existence of two sequences of constants,  $\{\sigma_n > 0\}$  and  $\{\mu_n\}$ , such that  $M_n^* = \frac{M_n - \mu_n}{\sigma_n}$ , rather than  $M_n$ , has a nondegenerate limit distribution  $G(x)$ :

$$P\{M_n^* < x\} \xrightarrow{w} G(x) \quad (\text{A4})$$

for each continuity point  $x$  of  $G$ .

**Theorem A.1 (Extremal Types Theorem).** *If there exist sequences of constant  $\{\sigma_n > 0\}$  and  $\{\mu_n\}$  such that the limit in (A4) exists, then the d.f.  $G(x)$  belongs to one of the following three parametric forms, called Extreme Value Distributions:*

$$\text{Type I (Gumbel): } G_1(x) = \exp \left\{ -\exp \left[ -\left( \frac{x - \mu}{\sigma} \right) \right] \right\}, \quad -\infty < x < +\infty \quad (\text{A5})$$

$$\text{Type II (Fréchet): } G_2(x) = \begin{cases} 0 & x \leq \mu, \\ \exp \left\{ -\left( \frac{x - \mu}{\sigma} \right)^{-\xi} \right\} & x > \mu, \quad \xi > 0 \end{cases} \quad (\text{A6})$$

$$\text{Type III (Weibull): } G_3(x) = \begin{cases} \exp \left\{ -\left[ -\left( \frac{x - \mu}{\sigma} \right) \right]^\xi \right\} & x < \mu, \quad \xi < 0 \\ 1 & x \geq \mu \end{cases} \quad (\text{A7})$$

with scale parameter  $\sigma > 0$ , location parameter  $\mu \in \mathbb{R}$  and, for the types II and III, the shape parameter  $\xi \neq 0$  (for type I it is assumed  $\xi = 0$ ).



This result was first proved by Fisher and Tippett [9] and then it was extended by Gnedenko [11]. The strength of this theorem is the fact that it is a *universal* property, since it holds regardless of the parent distribution  $F_X$ . Notice that:

- Theorem A.1 does not guarantee the convergence in distribution for the variable  $M_n^*$ . In fact it *assumes* it (compare (A4)). There are distributions for which the convergence requested in (A4) does not hold, see [29].
- The value of  $x_+$  is finite only for the Weibull distribution, whereas the Fréchet and Gumbel densities decay polynomially and exponentially as  $x \rightarrow +\infty$ , respectively.
- The *domain of attraction*  $D(G_i)$ , where  $G_i$  is one of (A5)-(A7), is defined as the set of all d.f.  $F(x)$  such that one has convergence to  $G_i(x)$  in (A4). Various criteria give necessary and sufficient conditions to determine what is the domain of attraction of each of the extremal distributions (A5)-(A7). However, the limit type for a given  $F(x)$  only depends on the *upper tail* of  $F(x)$ . See [29].
- The hypotheses of Theorem A.1 can be relaxed to the case of stationary stochastic processes with *weak long-range* dependence (at extreme levels) [5, Chap. 5], which is of particular importance in our case.

The Gumbel, Fréchet and Weibull families are unified into the single GEV family of distribution functions, given in (1). So in the sequel we denote by  $G(x)$  the family in (1). For positive values of the shape parameter  $\xi$ , the Fréchet family is obtained from (1) and, similarly, for negative values we have Weibull. The Gumbel distribution is the limit for  $\xi \rightarrow 0$  of  $G(x)$ :

$$\lim_{\xi \rightarrow 0} G(x) = \exp \left\{ - \exp \left[ - \left( \frac{x - \mu}{\sigma} \right) \right] \right\}. \quad (\text{A8})$$

This highlights another strength of the GEV model in concrete applications: the limit type is *inferred from the data* by estimating the parameter  $\xi$ . This removes the necessity of an initial and arbitrary choice of the limit type when using models (A5)-(A7).

## APPENDIX B: A MODEL FOR THE MID-LATITUDES ATMOSPHERIC CIRCULATION

As mentioned in the introduction, the *stochastic generator* of the energy time series used in this paper is a model for the baroclinic jet at mid-latitudes. The system is relaxed towards a prescribed north-south temperature profile, where the gradient is controlled by a parameter  $T_E$ . In fact, the parameter  $T_E$  controls average baroclinicity of the system and is used to study the relation with extreme values of the energy time series. Many dynamical properties of the model depending on  $T_E$  have been analyzed before the analysis of extreme values presented in this paper, providing a sort of *road map*. See [35, 36, 46], to which we also refer for a detailed derivation of the model and for discussion on the physics involved. In this section, we confine ourselves to a brief sketch.

Starting point for the construction of the model is the two-level quasi-geostrophic equation:

$$\begin{aligned} \frac{\partial}{\partial t} \Delta_H \tau - \frac{2}{H_2^2} \frac{\partial}{\partial t} \tau + J \left( \tau, \Delta_H \phi + \beta y + \frac{2}{H_2^2} \phi \right) + J(\phi, \Delta_H \tau) = \\ \frac{2\nu_E}{H_2^2} \Delta_H (\phi - \tau) - \frac{2\kappa}{H_2^2} \Delta_H \tau + \frac{2\nu_N}{H_2^2} (\tau - \tau^*), \end{aligned} \quad (\text{B1})$$

$$\frac{\partial}{\partial t} \Delta_H \phi + J(\phi, \Delta_H \phi + \beta y) + J(\tau, \Delta_H \tau) = -\frac{2\nu_E}{H_2^2} \Delta_H (\phi - \tau). \quad (\text{B2})$$

Here  $\tau$  and  $\phi$  are the baroclinic and barotropic components, respectively, of the streamfunction  $\psi_1$  and  $\psi_3$  at the two levels:

$$\tau = \frac{1}{2} (\psi_1 - \psi_3), \quad \phi = \frac{1}{2} (\psi_1 + \psi_3), \quad (\text{B3})$$

$\Delta_H$  is the horizontal Laplacian,  $1/H_2^2$  is the Froude number,  $\beta$  is the gradient of the Coriolis parameter,  $\nu_E$ ,  $\kappa$  and  $\nu_N$  parameterize the Ekman pumping at the lower surface, the heat diffusion, and the Newtonian cooling, respectively.

The system is driven for the baroclinic component by the term in  $(\tau - \tau^*)$  in (B1), which forces a relaxation to the radiative equilibrium  $\tau^*$  with a characteristic time scale of  $1/\nu_N$ . We take

$$\tau^* = \frac{R}{f_0} \frac{T_E}{4} \cos \left( \frac{\pi y}{L_y} \right), \quad (\text{B4})$$

so that  $T_E$  is the forced temperature difference between the low and the high latitude border of the domain. In this sense, the parameter  $T_E$  is responsible for average baroclinicity of the system and is the control parameter we vary to test changes in the extreme value statistics.

The fields  $\phi$  and  $\tau$  are expanded in Fourier series in the longitudinal direction  $x$ . Moreover, in order to avoid wave-wave nonlinear interactions, only the terms of order  $n = 1$  and  $n = 6$

are retained (see [35] for details). This yields

$$\phi(x, y, t) = - \int_0^y U(z, t) dz + A \exp(i\chi x) + \text{c.c.} \quad (\text{B5})$$

$$\tau(x, y, t) = - \int_0^y m(z, t) dz + B \exp(i\chi x) + \text{c.c.} \quad (\text{B6})$$

By substitution into (B1)-(B2), one obtains

$$\begin{aligned} \dot{A}_{yy} - \chi^2 \dot{A} + \left( i\chi U + \frac{2\nu_E}{H_2^2} \right) A_{yy} - \left( i\chi^3 U + i\chi U_{yy} + \frac{2\nu_E}{H_2^2} \chi^2 - i\chi\beta \right) A \\ + \left( i\chi m - \frac{2\nu_E}{H_2^2} \right) B_{yy} - \left( i\chi^3 m + i\chi m_{yy} - \frac{2\nu_E}{H_2^2} \chi^2 \right) B = 0, \end{aligned} \quad (\text{B7})$$

$$\begin{aligned} \dot{B}_{yy} - \chi^2 \dot{B} - \frac{2}{H_2^2} \dot{B} + \left( i\chi U + \frac{2\nu_E}{H_2^2} + \frac{2\kappa}{H_2^2} \right) B_{yy} \\ - \left( i\chi^3 U + i\chi U_{yy} + \frac{2\nu_E}{H_2^2} \chi^2 - i\chi\beta + \frac{2\kappa}{H_2^2} \chi^2 + \frac{2\nu_N}{H_2^2} + \frac{2}{H_2^2} i\chi U \right) B \\ + \left( i\chi m - \frac{2\nu_E}{H_2^2} \right) A_{yy} - \left( i\chi^3 m + i\chi m_{yy} - \frac{2\nu_E}{H_2^2} \chi^2 - \frac{2}{H_2^2} i\chi m \right) A = 0, \end{aligned} \quad (\text{B8})$$

$$\dot{U} + \frac{2\nu_E}{H_2^2} (U - m) + 2\chi \text{Im}(AA_{yy}^* + BB_{yy}^*) = 0, \quad (\text{B9})$$

$$\begin{aligned} \dot{m}_{yy} - \frac{2}{H_2^2} \dot{m} + \frac{2\kappa}{H_2^2} m_{yy} - \frac{2\nu_E}{H_2^2} (U - m)_{yy} - \frac{2\nu_N}{H_2^2} (m - m^*) \\ + \frac{4}{H_2^2} \chi \text{Im}(A^* B)_{yy} + 2\chi \text{Im}(AB_y^* + BA_y^*)_{yyy} = 0, \end{aligned} \quad (\text{B10})$$

where the dot indicates time differentiation and  $A^*$  denotes the complex conjugate of  $A$ . This is a set of 6 equations for the real fields  $A^1, A^2, B^1, B^2, U, m$ , where  $A^1$  and  $A^2$  are the real and imaginary parts of  $A$  and similarly for  $B$ . Rigid walls are taken as boundaries at  $y = 0, L_y$ , so that all fields have vanishing boundary conditions.

A system of ordinary differential equations is obtained from (B7)-(B10) by means of a pseudospectral (collocation) projection, involving a Fourier half-sine expansion of the fields of the form

$$A^i = \sum_{j=1}^{JT} A_j^i \sin\left(\frac{\pi j y}{L_y}\right), \quad i = 1, 2, \quad (\text{B11})$$

$$B^i = \sum_{j=1}^{JT} B_j^i \sin\left(\frac{\pi j y}{L_y}\right), \quad i = 1, 2, \quad (\text{B12})$$

$$U = \sum_{j=1}^{JT} U_j \sin\left(\frac{\pi j y}{L_y}\right), \quad (\text{B13})$$

$$m = \sum_{j=1}^{JT} m_j \sin\left(\frac{\pi j y}{L_y}\right). \quad (\text{B14})$$

The resulting system is the generator of the time series used in this paper for extreme value analysis. In particular, as *observable* (that is, as function of the state space yielding the

time series) we choose the total energy  $E(t)$  of the system, obtained by integration in the  $(x, y)$ -domain of the energy density:

$$e(x, y, t) = \frac{\delta p}{g} \left[ \frac{1}{2} \left( \vec{\nabla} \psi_1 \right)^2 + \frac{1}{2} \left( \vec{\nabla} \psi_3 \right)^2 + \frac{1}{2H_2^2} (\psi_1 - \psi_3)^2 \right]. \quad (\text{B15})$$

Here the factor  $\delta p/g$  is the mass per unit surface in each level, the first two terms inside the brackets describe the kinetic energy and the last term describes the potential energy. We emphasize that in the expression (B15) the potential energy term is half of what reported in [41], which contains a trivial algebraic mistake .

It turns out that the order  $JT = 32$  in the expansion (B11)-(B14) is sufficiently high to have an earth-like chaotic regime characterized by intermediate dimensionality in suitable ranges of the parameter  $T_E$ . By chaotic, we mean that the dynamics takes place on a strange attractor with internally generated noise. By earth-like we mean that the time-dependent Fourier coefficients in (B11)-(B14), as well as the total energy and mean zonal wind, have unimodal probability densities. The mentioned chaotic range is  $T_E > T_E^{crit}$ , where  $T_E^{crit} = 8.75$  approximately. For lower values of  $T_E$ , the Hadley equilibrium (stationary solution) is stable and is therefore the unique attractor. Again see [35, 36, 46] for a complete discussion. Throughout this work, we consider  $JT = 8, 16, 32$ , and 64 and the considered parameter range is  $10 \leq T_E \leq 50$  with integer steps of 2.

- 
- [1] A. Buzzi, A. Speranza: A theory of deep cyclogenesis in the lee of the Alps. Part II: Effects of finite topographic slope and height, *J. Atmos. Sci.*, **43** (1986), 2826–2837.
- [2] A. Buzzi, M. Fantini, P. Malguzzi, and F. Nerozzi: Validation of a limited area model in cases of Mediterranean cyclogenesis: Surface fields and precipitation scores, *Meteor. Atmos. Phys.*, **53** (1994), 137–153.
- [3] E. Castillo: Extreme Value Theory in Engineering, *Academic Press*, 1988.
- [4] J.G. Charney: The Dynamics of Long Waves in a Baroclinic Westerly Current, *J. Atmos. Sci.* **4** (1947), 136–162.
- [5] S. Coles: *An Introduction to Statistical Modelling of Extremes Values*, Springer Series in Statistics, Springer-Verlag London, 2001.
- [6] E.T. Eady: Long waves and cyclone waves, *Tellus* **1** (1949), 33–52.
- [7] J.-P. Eckmann, D. Ruelle: Ergodic theory of chaos and strange attractors, *Rev. Mod. Phys.* **57** (1985), 617–655.
- [8] P. Embrechts, C. Klüppelberg, T. Mikosch: *Modelling Extremal Events for Insurance and Finance*, 1st ed., Stochastic Modelling and Applied Probability **33**, Springer, 1997.
- [9] R.A. Fisher, L.H.C. Tippett: Limiting Forms of the Frequency Distribution of the Largest or Smallest Number of a Sample, *Proc. Cambridge Phil. Soc.* **24** (1928), 108–190
- [10] J. Galambos: *The Asymptotic Theory of Extreme Order Statistics*, Wiley, New York, 1978.
- [11] B.V. Gnedenko: Sur la distribution limite du terme maximum d’une série aléatoire, *Ann. Math* **44** (1943), 423–453.
- [12] I.M. Held, A.Y. Hou: Nonlinear Axially Symmetric Circulations in a Nearly Inviscid Atmosphere, *J. Atmos. Sci.* **37** (1980), 515–533.
- [13] J.R. Holton: *An Introduction to Dynamic Meteorology*. Academic Press, San Diego, 1992.
- [14] R. Ihaka, R. Gentleman: R: A language for data analysis and graphics, *Journal of Computational and Graphical Statistics*, **5(3)** (1996), 299–314.
- [15] Intergovernmental panel on Climate Change, Report: *Climate Change 2001: Impacts, Adaptation and Vulnerability*, [www.ipcc.ch](http://www.ipcc.ch).
- [16] Intergovernmental panel on Climate Change, Workshop Report *IPCC Workshop on Changes in Extreme Weather and Climate Events* Beijing, China, 11–13 June, 2002, [www.ipcc.ch](http://www.ipcc.ch).
- [17] T. Iwashima, R. Yamamoto: A statistical analysis of the extreme events: Long-term trend of heavy daily precipitation, *Journal of the Meteorological Society of Japan* **71** (1993), 637–640.

- [18] H. Jeffreys: On the Formation of Waves by Wind, *Proc. Roy. Soc. Lond.* **107** (1924), 189–206.
- [19] H. Jeffreys: On the Formation of Waves by Wind, *Proc. Roy. Soc. Lond.*, **110A** (1925), 341–347.
- [20] A.F. Jenkinson: The frequency distribution of the annual maximum (or minimum) values of meteorological elements, *Quart. J. Roy. Meteor. Soc.* **87** (1955), 158–171.
- [21] T.R. Karl, R.W. Knight: The Chicago heat wave: how likely is a recurrence? *Bull. Amer. Meteor. Soc.* **78**, (1997) 1107–1119.
- [22] T.R. Karl, R.W. Knight: Secular trend of precipitation amount, frequency, and intensity in the United States. *Bull. Amer. Meteor. Soc.* **79**, (1998) 231–242.
- [23] T.R. Karl, R.W. Knight, D.R. Easterling, R.G. Quayle: Indices of climate change for the United States, *Bull. Amer. Meteor. Soc.* **77**, (1996) 279–292.
- [24] R.W. Katz, B.G. Brown: Extreme events in a changing climate: Variability is more important than averages, *Climatic Change* **21**, (1992) 289–302.
- [25] R.W. Katz, M.B. Parlange, P. Naveau: Statistics of extremes in hydrology, *Adv. Water Resour.*, **25** (2002), 1287–1304.
- [26] A.M.G. Klein Tank, G.P. Können: Trends in Indices of Daily Temperature and Precipitation Extremes in Europe, *J. Climate* **16** (2003), 1946–1999.
- [27] K.E. Kunkel, R.A. Pielke Jr., S.A. Changnon: Temporal fluctuations in weather and climate extremes that cause economic and human health impacts: A review, *Bull. Amer. Meteor. Soc.* **80** (1999), 1077–1098.
- [28] K.E. Kunkel, K. Andsager, D.R. Easterling: Long-term trends in extreme precipitation events over the conterminous United States, *J. Climate* **12** (1999), 2515–2527.
- [29] G. Lindgren, M. R. Leadbetter, H. Rootzén: *Extremes and Related Properties of Random Sequences and Processes*, Springer-Verlag, New York (1983).
- [30] P. Lionello, F. Dalan, E. Elvini: Cyclones in the Mediterranean Region: the present and the doubled CO<sub>2</sub> climate scenarios, *Clim. Res.* **22** (2002), 147–159.
- [31] E.N. Lorenz: Available potential energy and the maintenance of the general circulation, *Tellus* **7** (1955), 157–167.
- [32] E.N. Lorenz: Generation of available potential energy and the intensity of the general circulation, in *Dynamics of Climate*, R.L. Pfeffer ed., Pergamon, Tarrytown (1960), 86–92.
- [33] E.N. Lorenz: *The Nature and Theory of the General Circulation of the Atmosphere*, World Meteorol. Organ., Geneva, 1967.
- [34] V. Lucarini: Towards a definition of climate science, *Int. J. Environment and Pollution* **18**

- (2002), 409–414.
- [35] V. Lucarini, A. Speranza, R. Vitolo: Geometrical Properties of the Attractor of a Model of Intermediate Complexity of the Mid-Latitudes Atmospheric Circulation, preprint ArXiv, DOI:\protect\vrule width0pt\protect\href{http://arxiv.org/abs/physics/0511208}\{phys (2005).
  - [36] P. Malguzzi, A. Trevisan, A. Speranza: Statistic and Predictability for an intermediate dimensionality model of the baroclinic jet, *Annales Geophysicae* **8** (1990), 29–36.
  - [37] M. Margules: Die energie der Stürme, *Jahrb. Zentralanst. Meteor. Wien* **40** (1903), 1–26.
  - [38] S.J. Mason, P.R. Waylen, G.M. Mimmack, B. Rajaratnam, J.M. Harrison: Changes in extreme rainfall events in South Africa, *Climatic Change* **41** (1999), 249–257.
  - [39] W.D. Nordhaus: *Managing the Global Commons. The Economics of Climate Change*, MIT Press, Cambridge (MA), 1994.
  - [40] O. Perrin, H. Rootzen, R. Taessler: A discussion of statistical methods for estimation of extreme wind speeds, *Theoretical and Applied Climatology*, to appear (2005).
  - [41] J. Pedlosky: *Geophysical Fluid Dynamics*, 2nd ed., Springer-Verlag, New York, 1987.
  - [42] J.P. Peixoto, A.H. Oort: *Physics of Climate*, Am. Inst. of Phys., College Park, 1992.
  - [43] N. Plummer, M. James Salinger, N. Nicholls, R. Suppiah, K.J. Hennessy, R.M. Leighton, B. Trewin, C.M. Page, J.M. Lough: Changes in climate extremes over the Australian region and New Zealand during the twentieth century, *Climatic Change* **42** (1999), 183–202.
  - [44] N.A. Phillips: Energy transformations and meridional circulations associated with simple baroclinic waves in a two-level, quasi-geostrophic model, *Tellus* **6** (1954), 273–286.
  - [45] A. Speranza, A. Buzzi, A. Trevisan, P. Malguzzi: A theory of deep cyclogenesis in the lee of the Alps. Part I. Modification of baroclinic instability by localized topography, *J. Atmos. Sci.*, **42** (1985), 1521–1535.
  - [46] A. Speranza, P. Malguzzi: The statistical properties of a zonal jet in a baroclinic atmosphere: a semilinear approach. Part I: two-layer model atmosphere, *J. Atmos. Sci.* **48** (1988), 3046–3061.
  - [47] R. Suppiah, K.J. Hennessy: Trends in total rainfall, heavy rain events, and number of dry days in Australia, 1910–1990, *Intern. J. of Climatology* **18**(10) (1998), 1141–1164.
  - [48] X. Zhang, F.W. Zwiers, G. Li: Monte Carlo Experiment on the Detection of Trends in Extreme Values, *J. Climate* **17**, (2003) 1945–1952.
  - [49] F.W. Zwiers, V.V. Kharin: Changes in the Extremes of the Climate Simulated by CCC GCM2 under CO<sub>2</sub> Doubling, *J. Climate* **11**, (1998) 2200–2222.
  - [50] F.W. Zwiers, V.V. Kharin: Changes in the Extremes in an Ensemble of Transient Climate

Simulations with a Coupled Atmosphere-Ocean GCM *J. Climate* **13**, (2000) 3760–3788.



n	$\gamma_1$	$T_E^b$	$\gamma_2$
1000	$1.7310 \pm 0.0007$	18	$1.6019 \pm 0.0017$
300	$1.7311 \pm 0.0013$	18	$1.6017 \pm 0.0030$
100	$1.7219 \pm 0.0018$	17	$1.5982 \pm 0.0018$

TABLE I: Power law fits of the location parameter  $\mu$  as a function of  $T_E$  of the form  $\mu \propto T_E^\gamma$ , performed in two adjacent intervals of  $T_E$ . The number of used annual extremes is  $n$  and  $T_E^b$  is the value of  $T_E$  separating the two intervals. Compare with figure Fig. 8.

$n$	$T_E^{b1}$	$\gamma_1$	$T_E^{b2}$	$\gamma_2$
1000	15	$3.011 \pm 0.076$	22	$2.140 \pm 0.025$
300	14	$3.236 \pm 0.115$	22	$2.114 \pm 0.047$
100	14	$2.944 \pm 0.157$	24	$2.040 \pm 0.093$

TABLE II: Same as Tab. I for the scale parameter  $\sigma$ . Here the fits  $\sigma = T_e^{\gamma_1}$  and  $\sigma = T_e^{\gamma_2}$  hold for  $T_E$  such that  $T_E^{b1} \leq T_E \leq T_E^{b2}$  and  $T_E^{b2} \leq T_E \leq 50$ , respectively. No power law fit is found for  $T_E < T_E^{b1}$ . Compare with Fig. 9.

JT	$\gamma_1$	$T_E^b$	$\gamma_2$
64	$1.7346 \pm 0.0008$	15	$1.6027 \pm 0.0005$
32	$1.7310 \pm 0.0007$	18	$1.6019 \pm 0.0005$
16	$1.7027 \pm 0.0007$	18	$1.5982 \pm 0.0007$
8	$1.6794 \pm 0.0006$	22	$1.5977 \pm 0.0011$

TABLE III: Power law fits of the location parameter  $\mu$  as a function of  $T_E$  of the form  $\mu \propto T_E^\gamma$ .  $JT$  indicates the spectral resolution (number of Fourier modes) of the baroclinic model and  $T_E^b$  is the value of  $T_E$  dividing the two considered intervals, see text for details.

$JT$	$T_E^{b1}$	$\gamma_1$	$T_E^{b2}$	$\gamma_2$
64	18	$2.514 \pm 0.046$	32	$2.067 \pm 0.055$
32	15	$3.011 \pm 0.076$	22	$2.140 \pm 0.025$
16	15	$2.821 \pm 0.045$	26	$2.150 \pm 0.033$
8	17	$2.675 \pm 0.065$	26	$2.149 \pm 0.033$

TABLE IV: Same as Tab. III for the scale parameter  $\sigma \propto T_E^\gamma$ . The interval  $[T_E^{b1}, T_E^{b2}]$  is the range of validity of the the first power-law, having exponent  $\gamma_1$ . The point dividing the two considered intervals is  $T_E^{b2}$ . No power law is detected for  $T_E < T_E^{b1}$ .

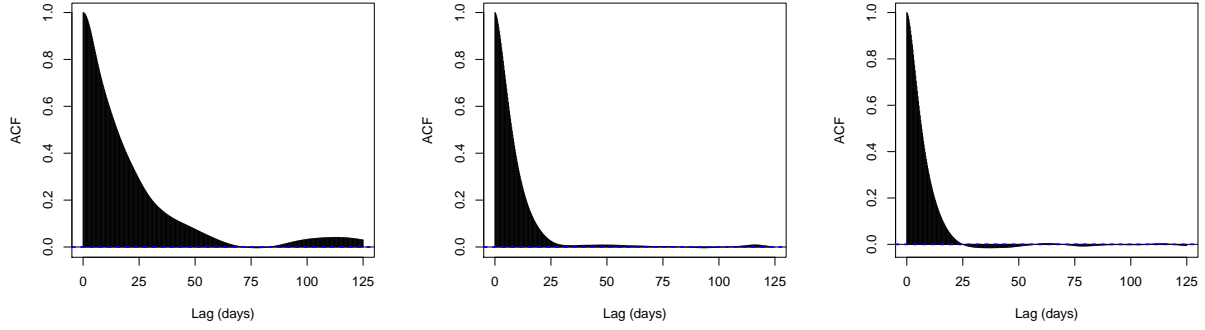


FIG. 1: Autocorrelations of the total energy time series for  $T_E = 10, 30, 50$  (left, center, right, respectively), time-lag in days on the horizontal axis. The full 6-hourly time-series of 1000 years have been used, see Sec. II A.

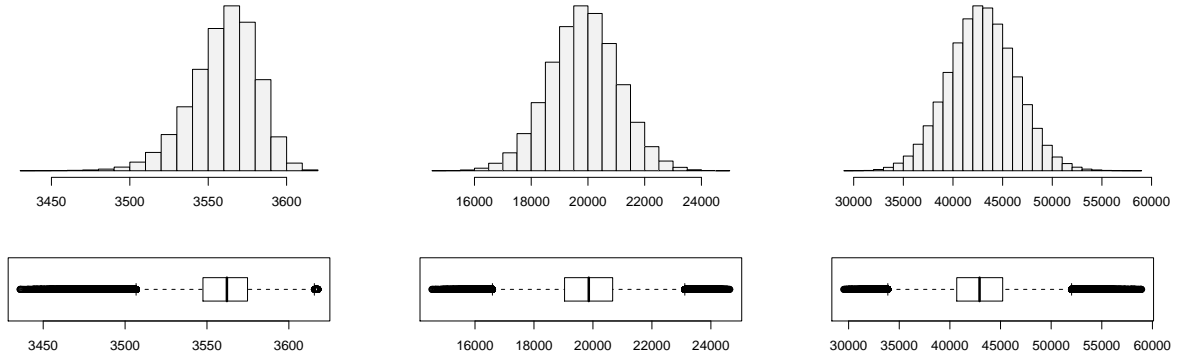


FIG. 2: Histograms and boxplots of the total energy time series for  $T_E = 10, 30, 50$  (left, center, right, respectively).

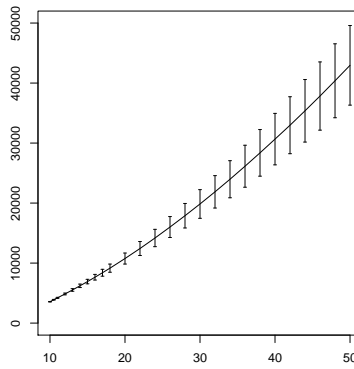


FIG. 3: Time-averaged total energy (vertical axis) as a function of  $T_E$  (horizontally), for each of the 21 selected values of  $T_E$ . Confidence bands (average plus or minus a 1.96 times sample standard deviation) are added. The full 6-hourly time-series of 1000 years have been used, see Sec. II A.

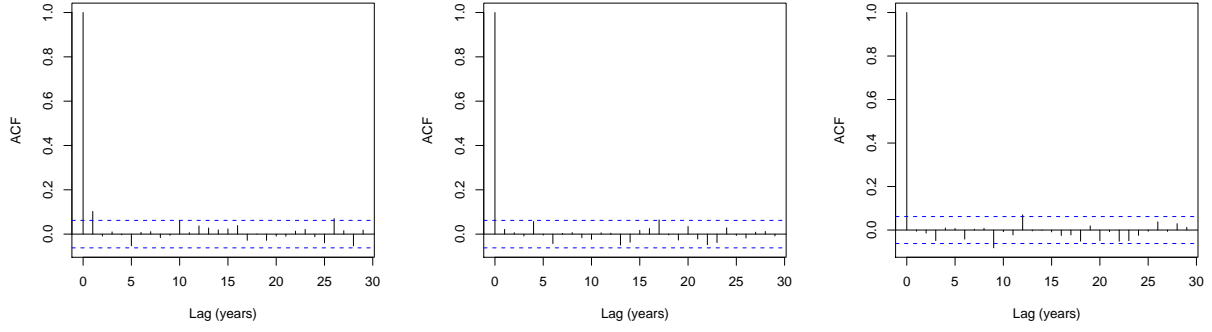


FIG. 4: Autocorrelations of the sequences of 1000 yearly maxima of the total energy time series for  $T_E = 10, 30, 50$  (from left to right, respectively).

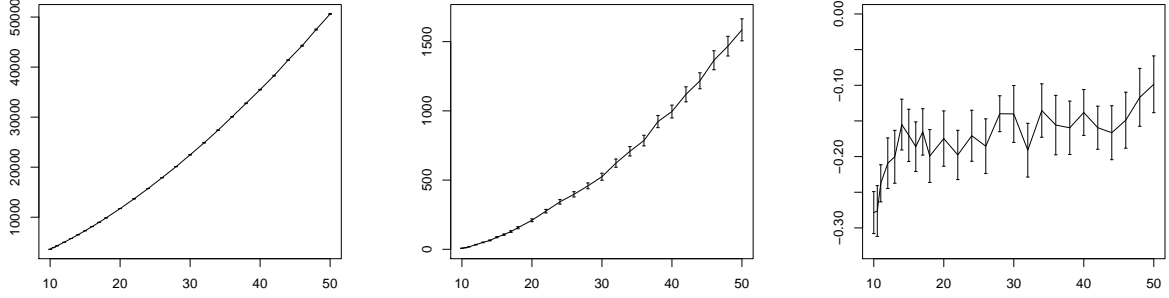


FIG. 5: From left to right: maximum likelihood estimates of  $\mu$ ,  $\sigma$ , and  $\xi$ , respectively (vertical axis), for each of the 21 sequences of 1000 maxima of the total energy, against the corresponding values of  $T_E$  (horizontal axis). Confidence intervals are added with errorbars but are hardly visible for  $\mu$  (leftmost panel) at the selected scale.

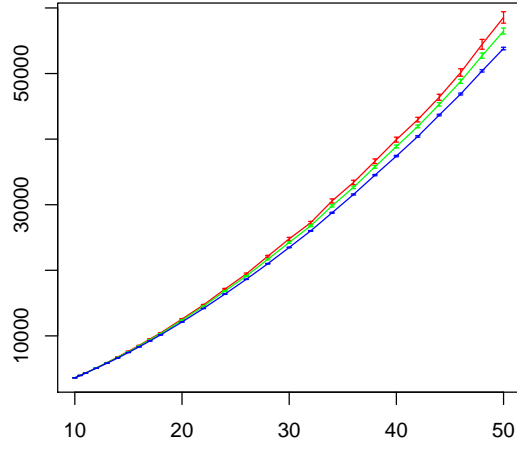


FIG. 6: Maximum likelihood estimates of the 10-, 100-, and 1000-year return levels of the total energy (red, green, and blue, respectively) for each of the 21 stationary series of 1000 maxima of the total energy, against the corresponding values of  $T_E$  (horizontal axis). Confidence intervals are added with errorbars but are hardly visible (at the selected scale).

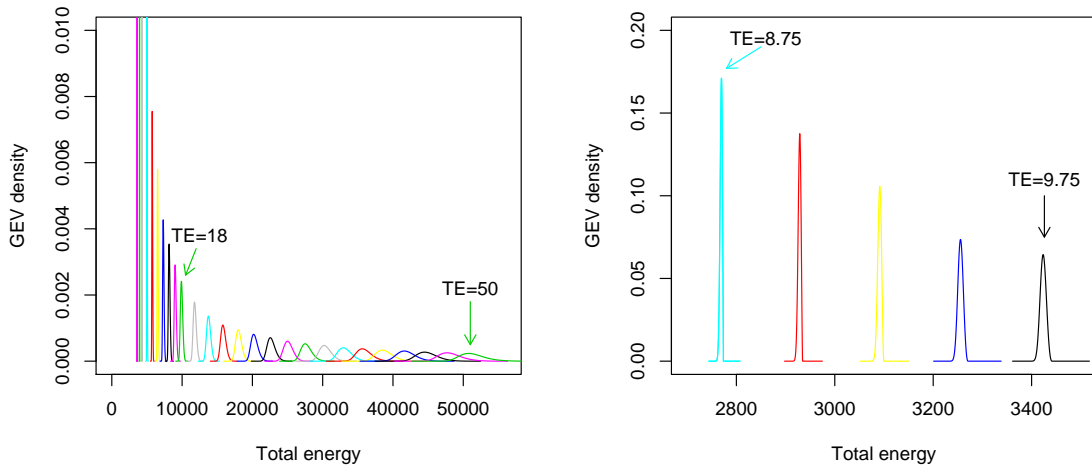


FIG. 7: Left: Probability density functions of the GEV for the 21 values of  $T_E$  in the considered range  $[10, 50]$ . Right: same as left for  $8.75 \leq T_E \leq 9.75$ .

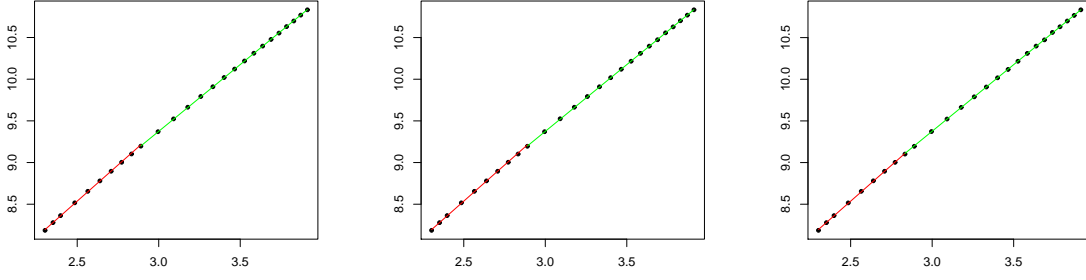


FIG. 8: Power law fits of the inferred values of  $\log(\mu)$  (vertical axis) as a function of  $\log(T_E)$  (horizontal axis). From left to right: 1000, 300, and 100 yearly maxima have been used. In each case, there are two intervals of  $T_E$ , separated by a point  $T_E^b$ , characterized by a different scaling exponent, compare Tab. I.

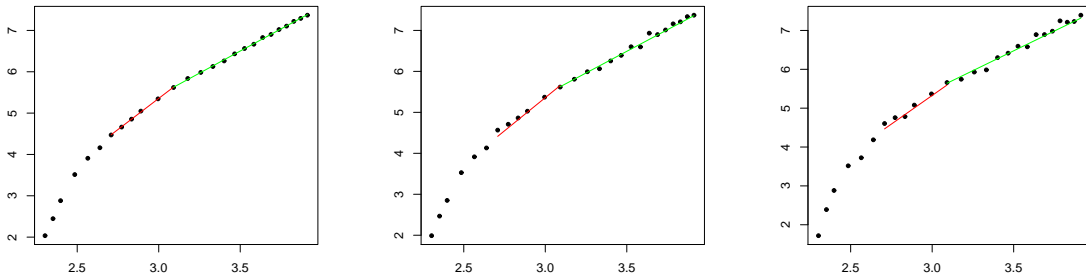


FIG. 9: Same as Fig. 8 for  $\log(\sigma)$ , see Tab. II.

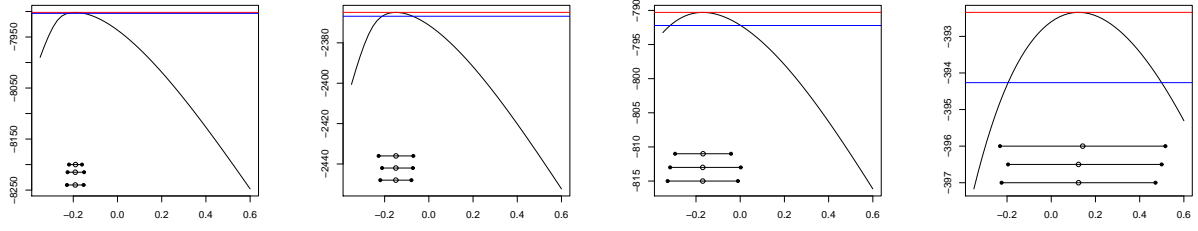


FIG. 10: Profile likelihood plots of  $\xi$  for  $T_E = 32$ . From left to right, 1000, 300, 100, and 50 yearly maxima have been used, respectively. In the latter case, the estimate of  $\xi$  is positive. Confidence intervals are computed by bootstrap, profile likelihood, and observed information matrix (the three stacked lines at the bottom part of the plots, from top to bottom, respectively). Notice the increasing width of the confidence intervals (quite large already for length 100) and the agreement between confidence intervals computed by the three methods, also for the *wrong* estimate obtained with 50 maxima.

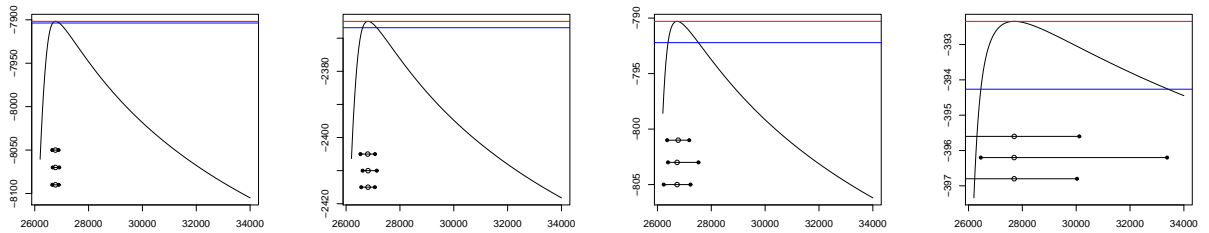


FIG. 11: Profile likelihood plots of the 100-year return level for  $T_E = 32$  for different lengths of the sample of yearly maxima: 1000, 300, 100, and 50 yearly maxima have been used from left to right, respectively. Confidence intervals are computed by bootstrap, profile likelihood, and observed information matrix (the three stacked lines at the bottom part of the plots, from top to bottom, respectively). Notice the increasing width of the confidence intervals and increasing skewness of those obtained by profile likelihood.

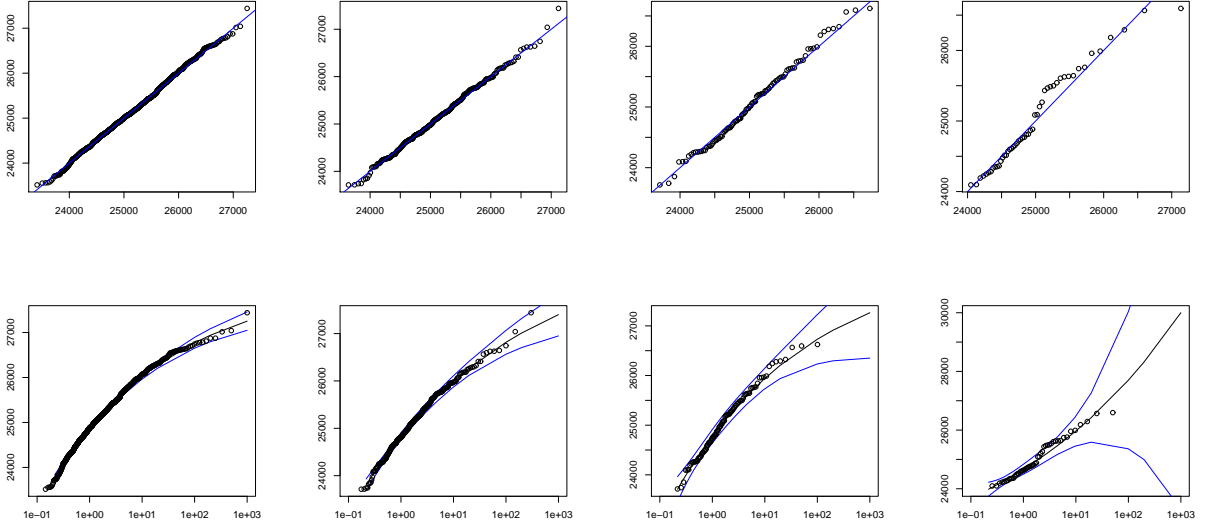


FIG. 12: Diagnostic plots of the GEV inferences for  $T_E = 32$ . Top and bottom row: quantile-quantile and return level plots, respectively (see Sec. II B for definitions). From left to right column: sequences of yearly maxima of the total energy are used, having lengths 1000, 300, 100, and 50, respectively. Notice the different scale of the vertical axis in the rightmost return level plot.



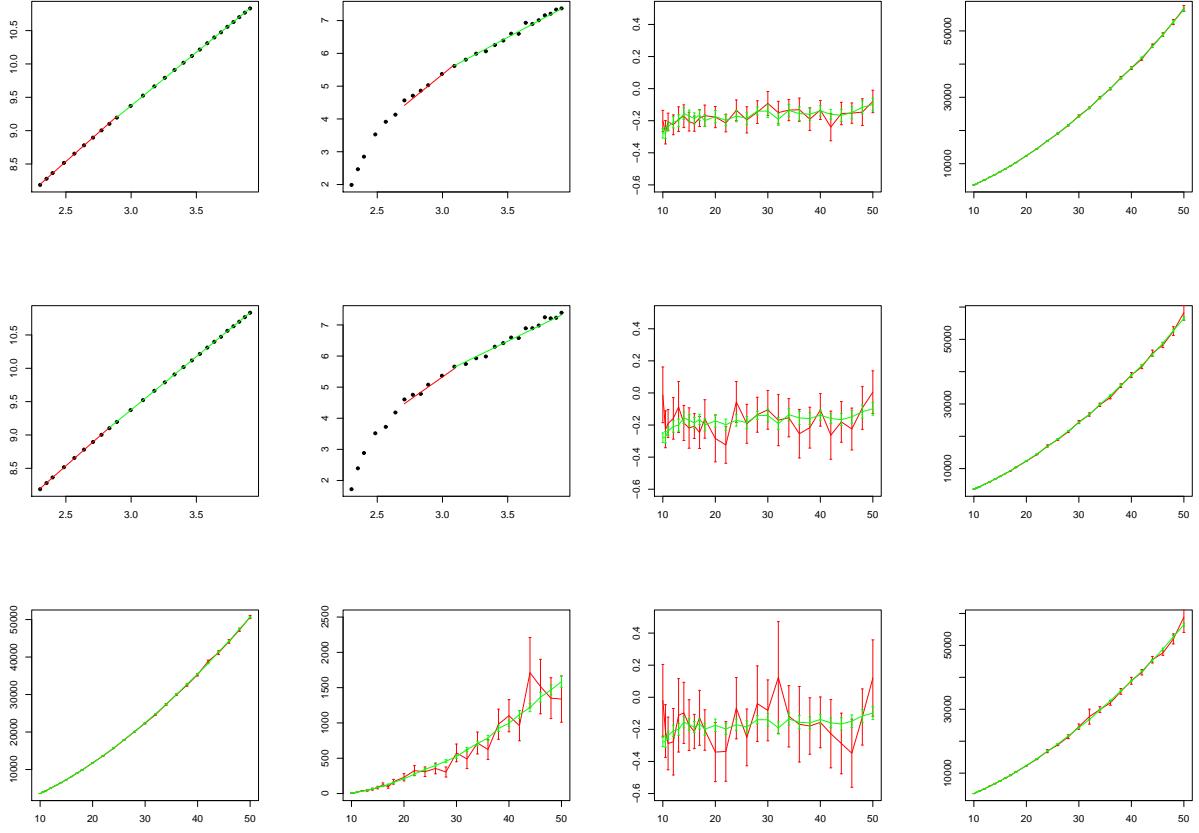


FIG. 13: Top row: maximum likelihood estimates of  $\mu$ ,  $\sigma$ , and  $\xi$  (from left to right, respectively) for 1000 and 300 yearly maxima (green and red respectively), with confidence intervals computed by the observed information matrix (7). Center, bottom row: same as top, for 100 and 50 yearly maxima, respectively, instead of 300. In the case of 50 maxima, for  $T_E = 32$  and 50 the inferred values of  $\xi$  are positive (thus completely wrong according to the theoretical expectation, see text) and the uncertainties are very large for  $\sigma$  and  $\xi$ .

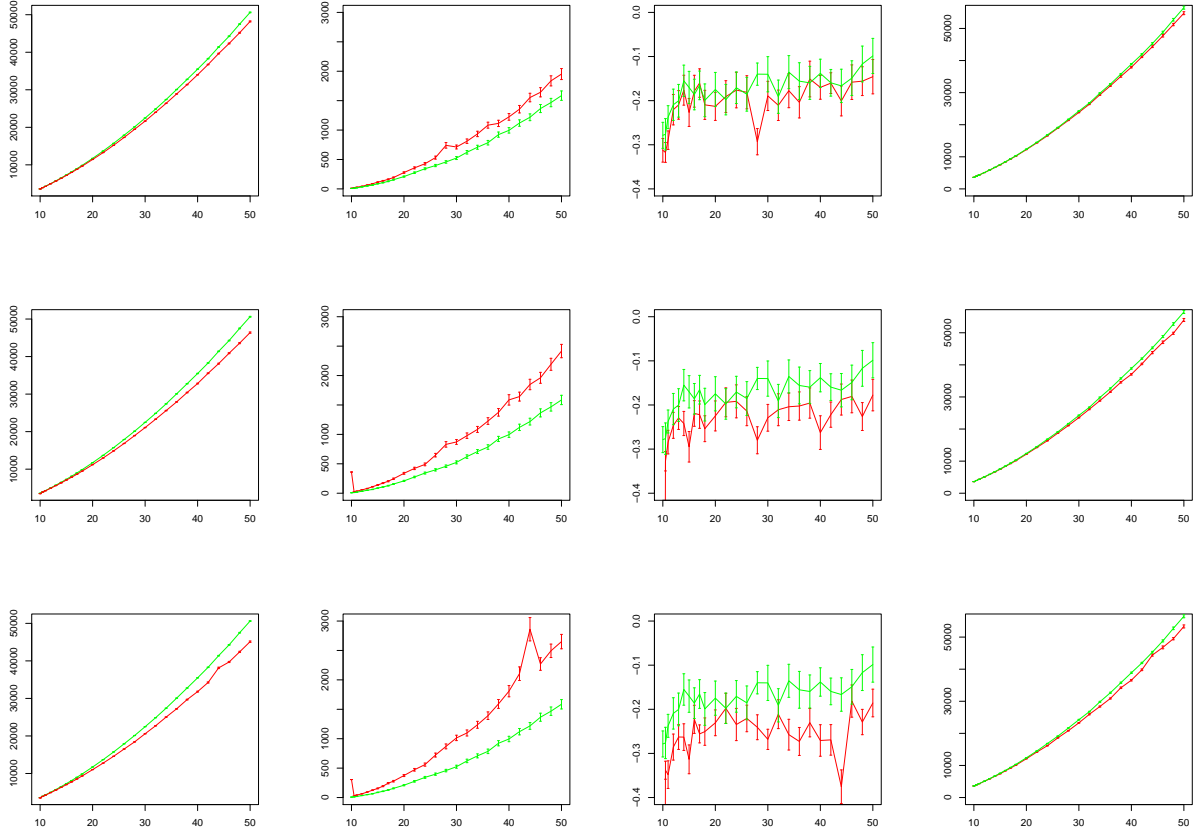


FIG. 14: Inferred values of GEV parameters as a function of  $T_E$  (horizontal axis) in a *soft extremes* experiment: from top to bottom row, sequences of 1000 maxima of the total energy time series are used, where the maxima are determined over data blocks corresponding to 3, 1.2, and 0.6 months. From left to right column,  $\mu$ ,  $\sigma$ ,  $\xi$ , and 100-year return levels are plotted. In green the estimates obtained for the yearly maxima (as in Fig. 5) are displayed for reference. Notice how the magnitude of the uncertainties shows little dependence on the temporal block length.

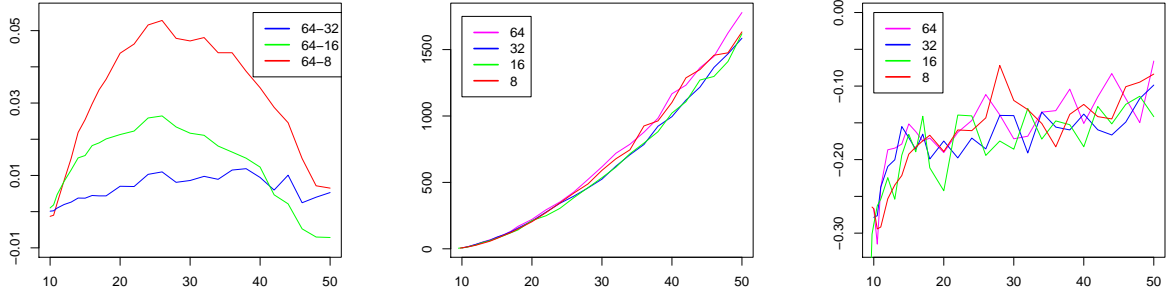


FIG. 15: Left: relative difference  $(\mu_{JT} - \mu_{64})/\mu_{64}$  of the maximum likelihood estimates of the GEV parameter  $\mu$  (vertical axis) for resolutions  $JT = 8, 16, 32$  (red, green, and blue, respectively) with respect to the reference case  $JT = 64$ . Middle, right: estimates of  $\sigma$  and  $\xi$ , respectively (vertical axis), for the cases  $JT = 8, 16, 32, 64$  (red, green, blue, magenta, respectively), where sequences of 1000 maxima are used. On the horizontal axis, the value of  $T_E$  is given for which the simulations are performed.